Molecular Therapy
Methods & Clinical Development
Original Article

Dose-response evaluation of intravenous gene therapy in a symptomatic mouse model of metachromatic leukodystrophy

Emilie Audouard,[1] Nicolas Khefif,[1] Charlotte Mansat,[1] Océane Nelcha,[1] Elena-Gaia Banchi,[1] Camille Lupiet,[1] Dominique Farabos,[3] Antonin Lamaziere,[3] Caroline Sevin,[1,2] and Françoise Piguet[1]

[1]TIDU GENOV, Institut du Cerveau, ICM, Inserm U 1127, CNRS UMR 7225, Sorbonne Université, 75013 Paris, France; [2]Bicêtre Hospital, Neuropediatrics Unit, Le Kremlin Bicêtre, 94275 Paris, France; [3]Sorbonne Université, Saint Antoine Research Center, INSERM UMR 938, Département de Métabolomique Clinique, Hôpital Saint Antoine, AP-HP Sorbonne Université, 75012 Paris, France

Metachromatic leukodystrophy (MLD) is a rare, autosomal recessive neurodegenerative disease caused by deficient activity of the lysosomal enzyme arylsulfatase A (ARSA), resulting in sulfatide accumulation and subsequent demyelination and neuronal damage within the central and peripheral nervous systems. Three clinical forms of MLD have been described, based on age at symptom onset. The most frequent and severe forms have an early onset, with the disease progressing rapidly toward severe motor and cognitive regression and ultimately premature death. There are currently no approved therapies for most of these early-onset patients once symptoms are present. Thus, it is crucial to develop new approaches to treat symptomatic patients. Here, we proposed a gene therapy approach based on the intravenous delivery of AAVPHP.eB encoding ARSA. MLD mice were treated at 6 months for a dose-response study and at 9 months to assess late-treatment efficacy. Therapeutic efficacy was evaluated 3 or 6 months after injection. We demonstrated a broad transduction in the central nervous system, a complete correction of sulfatide storage, and a significant improvement in neuroinflammation at low dose and late treatment. Taken together, this work establishes a strong rationale for proposing a phase I/II clinical trial in MLD patients.

INTRODUCTION

Metachromatic leukodystrophy (MLD) is an autosomal recessive inherited lysosomal storage disorder (LSD) caused by a deficiency of arylsulfatase A (ARSA; EC 3.1.6.8). The lysosomal enzyme ARSA catalyzes the degradation of galactosyl-3-sulfate ceramide (sulfatide), a major myelin sphingolipid.[1] The disease is characterized by myelin degeneration in both the central nervous system (CNS) and the peripheral nervous system (PNS), clinically resulting in progressive motor and cognitive impairments leading to premature death.[2] Three clinical forms are distinguished, based on the age of symptom onset: late infantile (LI; age of onset before 30 months); juvenile, subdivided into early juvenile (EJ; between 2.5 and 7 years) and late juvenile (LJ; between 7 and 16 years); and adult forms (after 16 years).[3,4] Levels of residual ARSA activity correlate with the type and severity of symptoms.[4] The most frequent and severe forms of MLD are early-onset forms, i.e., LI and EJ.[3] These patients develop neurological symptoms, including gait disturbance and loss of speech, around 2 years of age and die within a few years after symptom onset. Currently, there is no approved therapy to stop or delay disease progression once patients are symptomatic.[5] However, three approaches are investigated in clinical trials or even obtained EMA (European Medicines Agency) approval: intrathecal enzyme replacement therapy (IT-ERT),[6] *ex vivo* gene therapy based on the auto-transplantation of lentiviral vector-modified hematopoietic stem cells (HSC-GTs),[7–9] and adeno-associated virus-based gene therapy.[10] ERT is a good option[11]; however, ARSA does not efficiently cross the blood-brain barrier (BBB). Although results obtained *in vitro* and in MLD mice suggest that ARSA is able to cross the BBB to some extent,[12,13] the inefficient crossing hampers the appropriate delivery to the brain by intravenous injection, so intrathecal delivery is required. Results of a phase I-II trial, performed in early-symptomatic LI-MLD patients, confirmed a good safety profile, and for patients who received the highest dose (100 mg every 2 weeks), a normalization of the sulfatide content in the cerebrospinal fluid (CSF) has been shown, as well as a trend to a lesser decline in motor functions over time despite degradation.[6]

Ex vivo gene therapy is currently the gold standard treatment for pre-symptomatic MLD patients.[14] A clinical trial using autologous hematopoietic stem cell transplantation of CD34 cells corrected with a lentiviral vector overexpressing human ARSA (HSCT-GT; hARSA) showed very encouraging results in pre-symptomatic LI-MLD patients and pre- or early-symptomatic EJ-MLD patients (NCT01560182) and led to EMA approval of Libmeldy. However, this treatment was not efficient in symptomatic patients.[7,8] *Ex vivo* gene therapy has a significant clinical benefit in pre-symptomatic

Received 9 August 2023; accepted 3 April 2024;
https://doi.org/10.1016/j.omtm.2024.101248.

Correspondence: Françoise Piguet, TIDU GENOV, Institut du Cerveau, ICM, Inserm U 1127, CNRS UMR 7225, Sorbonne Université, F-75013 Paris, France.
E-mail: francoise.piguet@icm-institute.org

patients with early-onset forms of MLD, i.e., pre-symptomatic LI patients and pre- or early-symptomatic EJ patients. Limbeldy (Orchard Therapeutics) has obtained marketing authorization in the EU and is already available in some countries for pre-symptomatic LI and EJ patients and early-symptomatic EJ patients, while it is still under evaluation in a clinical trial for LJ patients.

In vivo gene therapy is another potential strategy for restoring hARSA expression *in vivo* by using an adeno-associated vector (AAV). An AAV can be administered directly in the CNS to avoid the obstacle of the BBB,[15] and previous studies have demonstrated its efficacy using an AAV5 or AAVrh10 to express hARSA in MLD mice,[16–18] as well as in non-human primates for scale-up studies.[19,20] A phase I/II clinical trial was initiated in four MLD children (aged between 9 months and 5 years, either pre-symptomatic or early-symptomatic), using intracerebral delivery of AAVrh10-hARSA (NCT01801709). Lessons of this trial were that intracerebral delivery is insufficient to achieve sufficient ARSA activity rescue in the CNS and that only targeting the brain is not sufficient to stop disease progression. Recently, Miyake et al. showed a reduction in sulfatide storage and neuroinflammation in the CNS after the intrathecal administration of an AAV9/ARSA vector in 6-week-old and 1-year-old MLD mice models. Intrathecal administration could be a promising approach for the treatment of MLD, although it may be essential to begin therapy before the onset of neurological symptoms.[21]

Recently, new AAV serotypes have emerged, such as AAV-PHP.eB, which was found to efficiently cross the BBB after intravenous delivery, leading to an efficient brain and spinal cord transduction in mouse models.[22] A previous study showed that a single intravenous injection of an AAVPHP.eB-hARSA-HA vector in 6-month-old MLD mice was effective in correcting, within 3 months, the sulfatide accumulation and the neuropathology in the brain and spinal cord.[23]

In this study, we evaluated the efficacy of long-term treatment, i.e., 6 months after the intravenous administration of an AAVPHP.eB-hARSA-HA vector, with a dose-response study. Additionally, we injected this vector into older mice (9 months of age) to assess the effect of the treatment once the symptoms were more advanced, which better reflects the situation of patients at the time of diagnosis. Our positive results allow us to move toward scale-up studies in large animals in order to propose a phase I/II study in symptomatic MLD patients. Even though previously published data revealed the absence of the Ly6 receptor in non-human primates (NHPs),[24,25] we demonstrated successful BBB crossing of AAVPHP.eB in NHPs.[26]

RESULTS

Characterization of the neuropathology of MLD mice at 6 and 9 months of age

Two parameters characterized the pathophysiology of MLD mice: sulfatide storage and neuroinflammation.[16–18] In the literature, sulfatide storage in MLD mice was observed at 6 months in the nervous systems, kidneys, and gallbladder.[27] The neuroinflammation (astrogliosis and microgliosis) in MLD mice was correlated with the degree of sulfatide storage.[28,29] Nevertheless, no quantification over time has been performed for these parameters.

Thus, we characterized sulfatide storage and neuroinflammation in wild-type (WT) and MLD mice at 6 and 9 months of age to describe the situation at the time of treatment delivery. Characterization was performed in the CNS and the PNS. At 6 months, sulfatide accumulation was observed in the CNS, sciatic nerve, gallbladder, and kidneys of MLD mice. At this time, the number of sulfatide storage inclusions was significantly increased in the cerebellar white matter, spinal cord, sciatic nerve, gallbladder, and kidneys of MLD mice compared with WT mice. Sulfatides began to accumulate in these structures and then spread to other brain areas. Over time, there is not only an increasing number of sulfatide inclusions but also an increase in the intensity of the staining of the aggregates, likely due to higher amounts of sulfatides present in the aggregates (notably in the kidneys), which was observed in all the analyzed tissues of 9-month-old MLD mice (Figure S2).

Neuroinflammation, characterized by microglia activation and astrogliosis and another classical hallmark of the disease, was already well established at 6 months. Microglial cells were significantly increased in the cerebellar white matter and corpus callosum of 6-month-old MLD mice compared with their WT littermates, and only a non-significant trend toward increased numbers was observed in the fimbria and spinal cord of these mice. At 9 months of age, the difference between WT and MLD mice was more marked (Figure S3). Astrogliosis was significantly increased in the cerebral cortex, cerebellar white matter, and spinal cord of 6-month-old and 9-month-old MLD mice compared with WT mice. A trend toward higher astrogliosis was also observed in the corpus callosum and fimbria, although it was less pronounced than in the other brain areas (Figure S4). Neuroinflammation was confirmed to be present in the CNS of MLD mice at 6 months of age and to worsen from 6 to 9 months. Thus, we can regard the 6-month-old MLD mice cohort as symptomatic MLD and the 9-month-old cohort as late-symptomatic MLD.

Intravenous administration of an AAVPHP.eB-hARSA-HA vector led to the widespread distribution and expression of the vector and recombinant enzyme in the CNS of knockout ARSA mice

Early- and late-treated MLD mice (i.e., 6 or 9 months old, respectively; $n = 6$ to 12) received a single retro-orbital intravenous injection of AAVPHP.eB-hARSA-HA at a dose of 2.5×10^{11} (named dose 1) or 5×10^{11} (dose 2) vg total (Figure S1B). As shown in our previous study,[23] AAVPHP.eB-hARSA-HA resulted in a widespread transduction in the CNS (Figure 1A) and a weak peripheral transduction. The biodistribution was similar in early- and late-treated mice, and no dose-response effect was observed at 6 months of treatment (no statistical difference), except for the striatum, in which the vector genome copy (VGC) number increased significantly between dose 1 (3.6) and dose 2 (5.9; $p = 0.0437$). The mean VGC number was less than 0.15 in the liver and was below 0.025 in all other peripheral

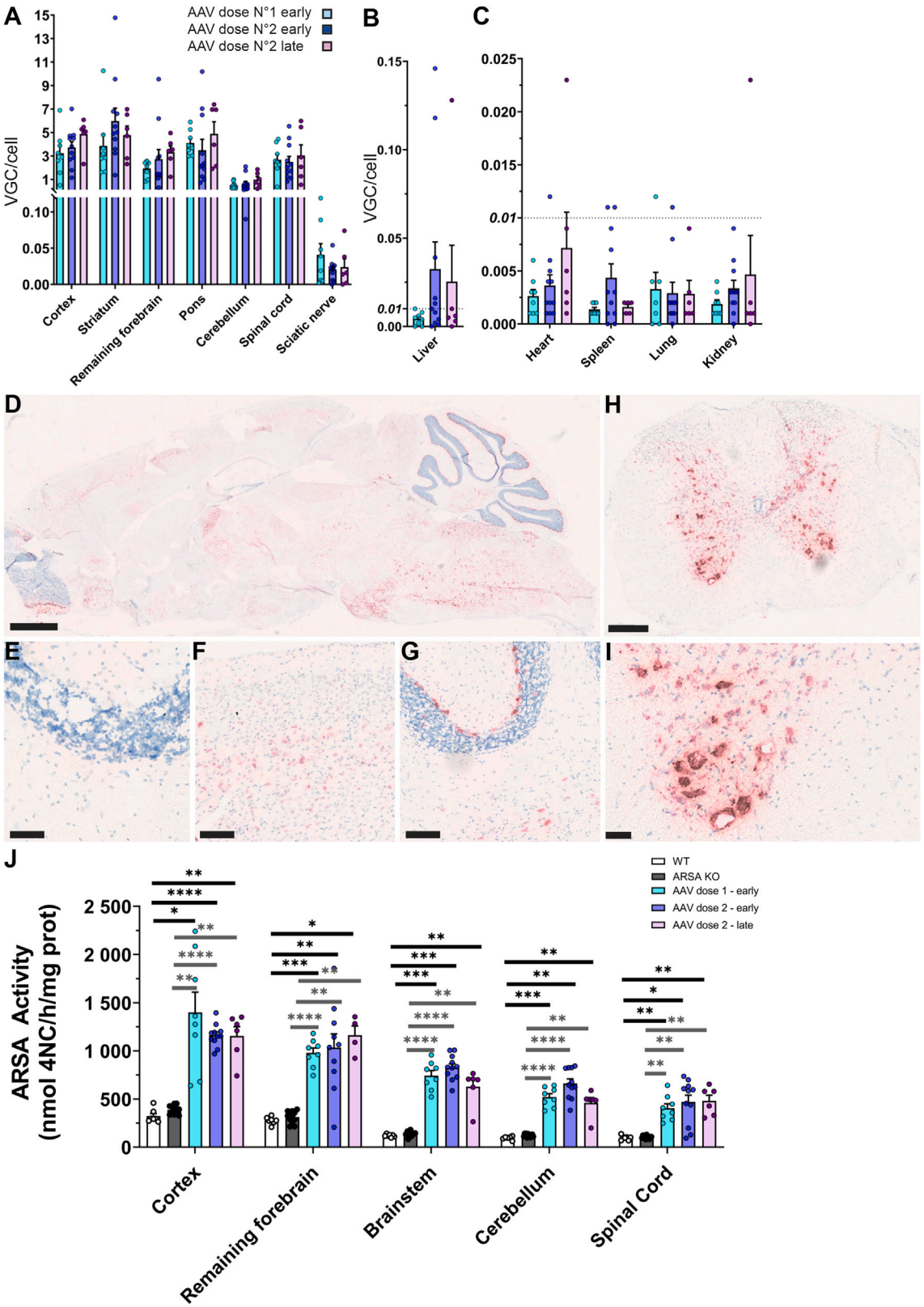

(legend on next page)

organs, indicating a low peripheral transduction of the vector (Figure 1B).

Consistent with the biodistribution pattern and according to a previous study,[23] hARSA-HA mRNA was detected using BaseScope technology in several brain areas (Figure 1C) of treated knockout (KO) ARSA mice, such as the striatum, hippocampus, thalamus, cerebral cortex (Figure 1E), pons, and cerebellum (Figure 1F). Moreover, hARSA-positive cells were also detected in the spinal cord (Figure 1G) of treated mice, with a particularly strong transduction in motor neurons (Figure 1H). As a negative control, hARSA-HA mRNA was not detected in untreated KO ARSA mice (Figure 1D).

Intravenous administration of an AAVPHP.eB-hARSA-HA vector led to a significant increase in hARSA activity in the CNS of treated MLD mice

To validate the functionality of the recombinant hARSA vector in treated KO ARSA mice, ARSA activity was measured in several structures of the CNS. We demonstrated a strong and sustained ARSA activity in the cortex and the rest of the brain (with an approximately 3-fold increase), the pons (with an approximately 5-fold increase), and the cerebellum and spinal cord (with an approximately 4-fold increase) in KO ARSA treated mice compared with WT and non-treated MLD mice. No obvious difference was observed between doses (i.e., dose 1 or 2) and the age at treatment (i.e., 6 or 9 months; Figure 1I). ARSA activity was similar in WT and untreated mice, as expected and previously described. Therefore, this increase in hARSA activity in treated mice was specific to the administration of the vector itself and reinforced the therapeutical potential of our AAVPHP.eB vector.

A significant improvement in MLD neuropathophysiology was observed in early- and late-symptomatic MLD mice after treatment

To assess the therapeutic efficiency, two hallmark criteria of the disease were analyzed, namely sulfatide storage and neuroinflammation. To assess whether the intravenous administration of an AAVPHP.eB-ARSA-HA vector could decrease sulfatide storage, we used two different methods: Alcian blue staining and gas chromatography-mass spectrometry (GC-MS) analysis. Alcian blue coloration was performed on the brain, spinal cord, sciatic nerve, gallbladder, and kidney sections of untreated and treated MLD mice and was compared with WT tissues. 12-month-old untreated MLD mice displayed massive sulfatide storage in the brain, spinal cord, sciatic nerve, gallbladder, and kidneys compared with WT mice (Figure 2; data not shown for the kidneys, gallbladder, and sciatic nerve). In early-treated mice, 6 months after intravenous injection, the AAVPHP.eB-ARSA-HA vector led to a complete rescue of the sulfatide storage in the brain and spinal cord of treated MLD mice (Figures 2B–2H, 2N, 2T, and 2Z). This was confirmed by the quantification of the number of sulfatide storage inclusions in the substructures of the brain and spinal cord (Figures 2F, 2L, 2R, 2X, and 2AD). No significant difference was observed between the two treatment doses, demonstrating that the low dose is still higher than the minimum effective dose and that it is sufficient to achieve a complete correction of sulfatide, so an increase in dose is not necessary. In late-treated animals, a significant decrease in the number of sulfatide inclusions was observed compared with untreated mice. It should be noted that for the late-treated mice, the correction was not complete, but the effect of the treatment was analyzed 3 months after treatment, thus demonstrating a strong potential of the treatment 3 months after the administration of the vector. These data were confirmed by GC-MS quantification of the sulfatide isoforms. GC-MS was performed only in the cerebellum and spinal cord samples of animals treated with dose 2 as this technique is expensive (Figures 3 and S5). In the CNS, there are several isoforms of sulfatides; C18 sulfatide is present mainly in neurons, while long-chain C22–C26 sulfatides are found in oligodendrocytes.[30] The amounts of sulfatide species were reduced in early- and late-treated mice, and both neuron-specific isoforms (C18:0) and oligodendrocyte-specific isoforms (C22–C26) were normalized. GC-MS quantifications demonstrated a complete correction of the sulfatide storage in the treated animals for all species of sulfatides (neuron and oligodendrocyte species) and for both early and late treatment with dose 2 (Figures 3 and S5).

Moreover, sulfatide storage was also reduced in the sciatic nerve of treated mice but not in the gallbladder and kidneys, which remained similar to that in untreated animals (data not shown). The VGC quantification in the kidneys demonstrated less than 0.01 in the kidneys (Figure 1B). VGC was not quantified in the gallbladder, which was studied only with histological analysis; however, previous data did not show any transduction of AAVPHP.eB in the gallbladder, so sulfatide data correlate with the absence of transduction in these two organs.

To assess the effect of AAVPHP.eB-hARSA-HA treatment on neuroinflammation in MLD mice, immunohistochemical staining was performed to evaluate astrogliosis and microgliosis in the brain and spinal cord sections of the different groups of mice. A significant increase in Iba1-and GFAP-positive cells was observed in the brain and spinal

Figure 1. AAVPHP.eB-hARSA-HA efficiently transduces the central nervous system

(A–C) Biodistribution of AAVPHP.eB-hARSA-HA in different brain structures, the spinal cord, a peripheral nerve (A), and peripheral organs (B and C) in 12-month-old KO ARSA mice, 3 or 6 months after intravenous injection. VGC number per 2*n* genome. (D–G) Localization and expression of hARSA mRNA (red) in sagittal sections of the brain (D) and high-magnification images of different brain areas (E–G), i.e., the cerebral cortex (F) and cerebellum (G), in 12-month-old KO ARSA mice treated with AAVPHP.eB-hARSA-HA (D, F, and G) and in 12-month-old untreated KO ARSA mice (E). (H and I) Localization and expression of hARSA mRNA (red) in transversal sections of the spinal cord (H) and a high-magnification image of the ventral spinal cord (I). (J) ARSA activity in several brain regions and the spinal cord in 12-month-old wild-type, untreated, and early- or late-treated KO ARSA mice treated with AAVPHP.eB-hARSA-HA. Data are presented as mean ± SEM. Scale bars: 1,000 μm (C), 250 μm (G), 100 μm (E and F), and 50 μm (D and H).

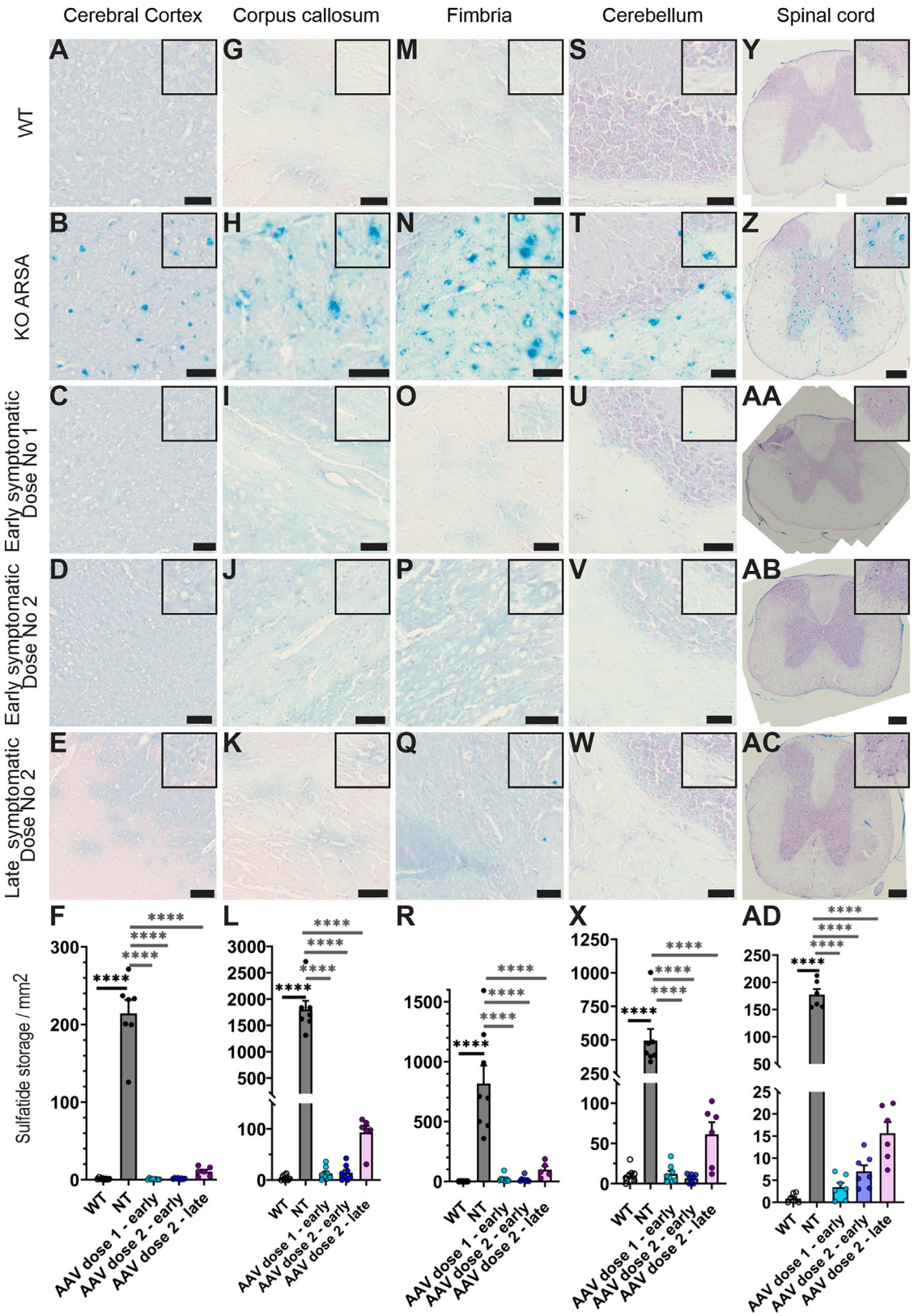

(legend on next page)

cord of untreated MLD mice at 12 months compared with WT mice (Figures 4 and 5). After early and late injection of the AAVPHP.eB-hARSA-HA vector, a significant and complete correction of microgliosis and astrogliosis was observed in the cerebral cortex, corpus callosum, fimbria, and spinal cord of treated mice (Figures 4 and 5). However, although improved, significant microgliosis and astrogliosis were still present in the cerebellum of treated mice compared with WT mice.

To conclude, a single administration of AAVPHP.eB-hARSA-HA in MLD mice showed a significant and almost complete correction of sulfatide accumulations in the nervous system (CNS and sciatic nerve) as well as much less neuroinflammation in the CNS of early- and late-treated MLD mice.

Massive macrophage recruitment near sulfatide accumulations

To better understand how treatment improves sulfatide storage, we performed Alcian blue staining concomitant with immunohistochemical analysis for CD-68 (macrophage marker) on the brain and spinal cord sections of the different groups of 12-month-old mice. In untreated mice, we observed a number of sulfatide accumulations (as shown in Figure 2) and also a large number of CD68-positive cells in the CNS. We quantified 70%–80% of sulfatide aggregates that co-localized with CD68-positive cells in the cortex, cerebellar white matter, and spinal cord and around 50% in the corpus callosum and fimbria (Table 1). This co-localization involved essentially large-size sulfatide inclusions (Figures 6A–6L). In treated MLD mice, we detected only a few or even no sulfatide aggregates in the CNS (as shown in Figure 2). Most of these inclusions were co-localized with CD68 staining. The number of CD68-positive cells was normalized in treated mice compared with untreated mice.

To further characterize these CD68-positive cells, Alcian blue coloration with double immunofluorescence staining for CD-68 and Iba1 was performed on the brain and spinal cord sections of all the animal cohorts. In untreated mice, a mean number of 38% sulfatide aggregates co-localized with both CD68- and Iba1-positive cells. In contrast, in treated mice, a mean number of 53%–75% of the remaining sulfatide aggregates co-localized with both CD68- and Iba1-positive cells depending on the brain region (Figures 6M–6X and Table 2). Recall that untreated mice exhibited severe CNS neuroinflammation, while treated mice had normal microgliosis (Figure 4). These results reveal that massive macrophage recruitment close to sulfatide aggregates in MLD mice is a cell response that tries to clear aggregates. These cells were not primarily Iba-positive cells but probably other immune cells. Restoring ARSA expression allowed the restoration of the sulfatide degradation pathway leading to the catabolization of sulfatide inclusions, most probably by microglial cells or at least support cells.

DISCUSSION

In MLD, a deficiency of the lysosomal ARSA enzyme results in sulfatide accumulation, affecting oligodendrocytes and leading to myelin loss in the CNS.[31] However, neurons are also subject to sulfatide storage.[31,32] Given the rapid and devastating progression of cerebral disease in patients with the LI form of MLD, the therapeutic challenge is to deliver rapidly and efficiently ARSA recombinant expression in both neurons and oligodendrocytes, not only in the brain but also in the spinal cord. This is particularly important in symptomatic LI-MLD patients, in whom the autologous HSC transplantation of corrected cells is not efficient.[8]

Different phase I/II trials are currently in progress in LI-MLD patients. One of these is ERT, which uses recombinant hARSA (called SHP611) delivered intrathecally to assess the effect of this treatment on diminishing the symptoms of the disease and to see how the treatment is tolerated when hARSA is injected directly in the CSF (NCT03771898). Another phase I/II trial has been carried out to evaluate the safety and efficacy of i.v. ERT with recombinant human ASA (rhASA; HGT-1111, previously known as Metazym) in MLD patients. The treatment was well tolerated in patients but was not sufficient to slow down the evolution of the disease, probably due to the fact that IV rhASA may not cross the BBB in therapeutic quantities (NCT00418561).[33] Despite these results, these approaches were not sufficient to abolish symptoms or to significantly improve patients' quality of life. More recently, Miyake et al. described an intrathecal approach of AAV9 in mice that alleviates sulfatide storage[21]; a similar approach was applied in minipigs.[34] However, such an approach in humans remained invasive, and intravenous AAV9 delivery in humans was recently found to be associated with severe adverse effects.[35–37]

Our study demonstrated that intravenous AAVPHP.eB-hARSA-HA administration in early- and late-symptomatic MLD mice led to a robust and complete correction of sulfatide storage in the brain and spinal cord, as in our previous study.[23] Our treatment allows a complete correction of sulfatide storage in the CNS, whereas the correction in the spinal cord of treated animals was never observed previously with both an AAV5 and an AAVrh10 intracerebral approach[16–18] and never reported in MLD mice after ERT.[13,38] Moreover, we observed similar results when the animals were injected at 6 or 9 months of age (i.e., only 3 months after treatment in late-affected

Figure 2. Correction of sulfatide storage in the brain and spinal cord of treated MLD mice, 3 or 6 months after treatment

(A–E, G–K, M–Q, S–W, Y–AC) Alcian blue staining in the cerebral cortex (A–E), corpus callosum (G–K), fimbria (M–Q), cerebellar white matter (S–W), and spinal cord (Y–AC) of wild-type mice (WT; A, G, M, S, and Y), untreated mice (KO ARSA; B, H, N, T, and Z), early-treated MLD mice with dose 1 (C, I, O, U, and AA) or dose 2 (D, J, P, V, and AB), and late-treated MLD mice with dose 2 (E, K, Q, W, and AC). Inserts are the high-magnification images of tissue sections to show the absence or the presence of sulfatide storage. (F, L, P, R, X, and AD) Quantification of sulfatide storage per mm^2 in the cortex (F), corpus callosum (L), fimbria (R), cerebellar white matter (X), and spinal cord (AD) of WT, untreated (NT), and early- or late-treated MLD mice. Data are presented as mean ± SEM. Scale bars: 50 μm, expect for (D), (E), and (U), which have a scale bar of 100 μm; spinal cord images have a scale bar of 200 μm. $^{****}p < 0.0001$.

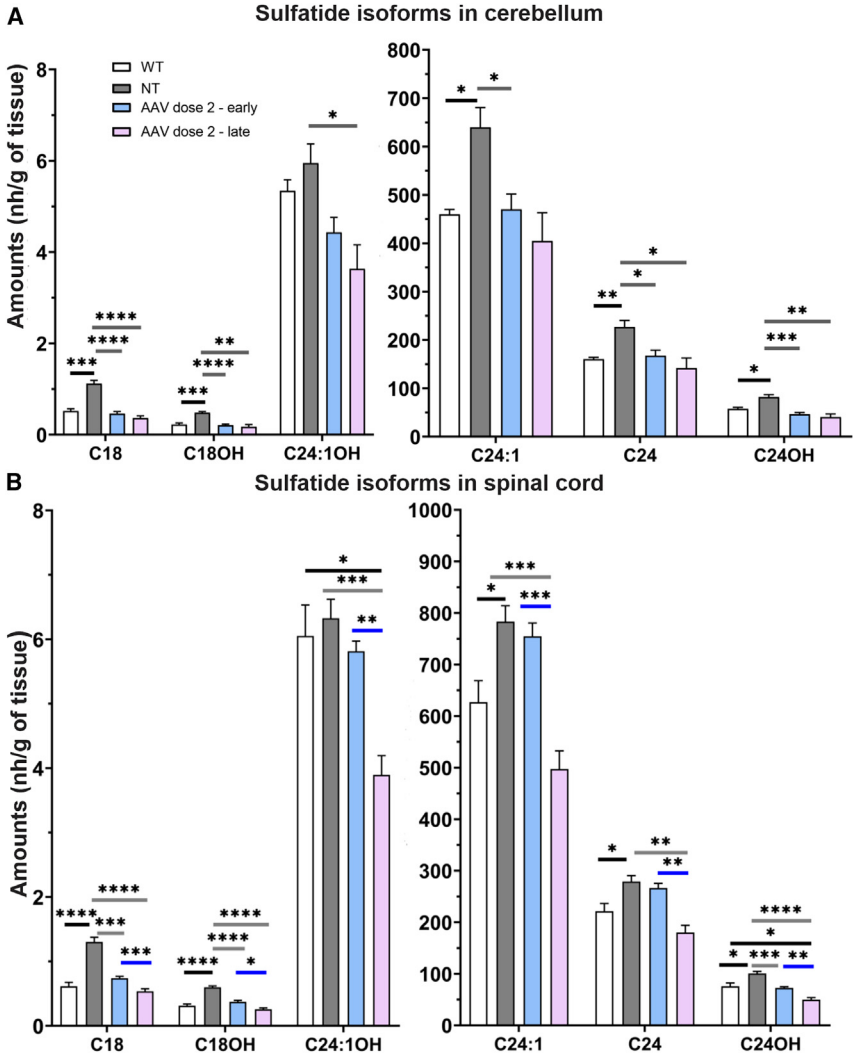

Figure 3. Evaluation of sulfatides isoform by gas spectroscopy

Correction of sulfatide isoforms (C18:0, 24:0) in the cerebellum (A) and spinal cord (B) of early- or late-treated MLD mice. Data are presented as mean ± SEM. $p < 0.05$; $^{**}p < 0.01$; $^{***}p < 0.005$; $^{****}p < 0.0001$.

mice), which has never been reported before.[23] The mice were treated at 6 months, an age at which sulfatide storage was already clearly detectable in the CNS and peripheral organs. The treatment efficiency was evaluated at 3 months (in a previous study) and 6 months after injection, and a complete rescue was observed. Similarly, we did not observe any differences depending on the dose injected in the treated animals. Other mice were treated at 9 months, an age at which sulfatide storage is strongly detectable in the CNS and peripheral organs. The therapeutic efficiency was assessed at 3 months after injection, and a significant rescue was observed. This rescue would certainly be better 6 months after treatment. This means a strong expression of ARSA leading to a rapid reversal of sulfatide storage, which is a crucial advantage for the rapidly progressive form of MLD. Our approach could treat both early- and late-symptomatic MLD patients.

To further characterize our treatment regarding sulfatide storage, we were interested in the correction of different isoforms of sulfatides. In the mouse model and its control, a general trend of an age-related (up to 4 months of age) increase in very long-chain fatty acids (C22–C26) and a decrease in short-chain fatty acids (C16–C20) was observed. Moreover, it is known that sulfatide C18 fatty acid, an isoform in neurons and astrocytes, increases in MLD mice at older age.[39] After treatment of early- and late-symptomatic MLD mice, a rescue of the amounts of sulfatide isoforms was observed in the cerebellum and spinal cord of all animals treated with dose 2 (not tested in animals treated with dose 1). This is a major breakthrough as our previous approach with intracerebral delivery of AAVrh10-ARSA demonstrated a correction of the sulfatide isoform only in the brain but never in the cerebellum and spinal cord.[17]

The second hallmark of the disease on which we focused was astrogliosis and microgliosis, for which we demonstrated a significant improvement in AAVPHP.eB-hARSA-HA-treated mice. Our treatment allows the normalization of neuroinflammation both in the brain and in the spinal cord, as previously shown,[23] even in animals treated with a low dose and in the late-treatment group. The AAV5 and AAVrh10 intracerebral approaches[16–18] and the ERT[13,38] never demonstrated such an improvement in neuroinflammation in the spinal cord of treated animals. Moreover, a massive recruitment of macrophages was observed close to sulfatide storages in MLD mice. CD68 is related to the LAMP family of glycoproteins; consequently, CD68 is mainly localized in endosomal or lysosomal compartments.[40,41] CD68 is highly expressed in macrophages and other mononuclear phagocytes.[42] Thus, it is normal to detect macrophages in MLD mice, as they play a critical role in neuroinflammation in various CNS disorders and are responsible for the clearance of cell debris and proteins at lesion sites.[43,44] Moreover, in order to better characterize these CD68-positive cells, we performed Alcian blue coloration followed by double immunofluorescence staining with anti-CD-68 and anti-Iba1 antibodies on brain and spinal cord sections. Most of these macrophages are not microglial cells; only 38% are $CD68^+/Iba1^+$ in MLD mice. Nevertheless, Iba1 is considered a pan-microglial marker.[45] Microglial cells are the resident macrophages of the brain and spinal cord and act as the main immune defense in the CNS. Waller et al. also found a population of $Iba^-/CD68^+$ microglial cells or

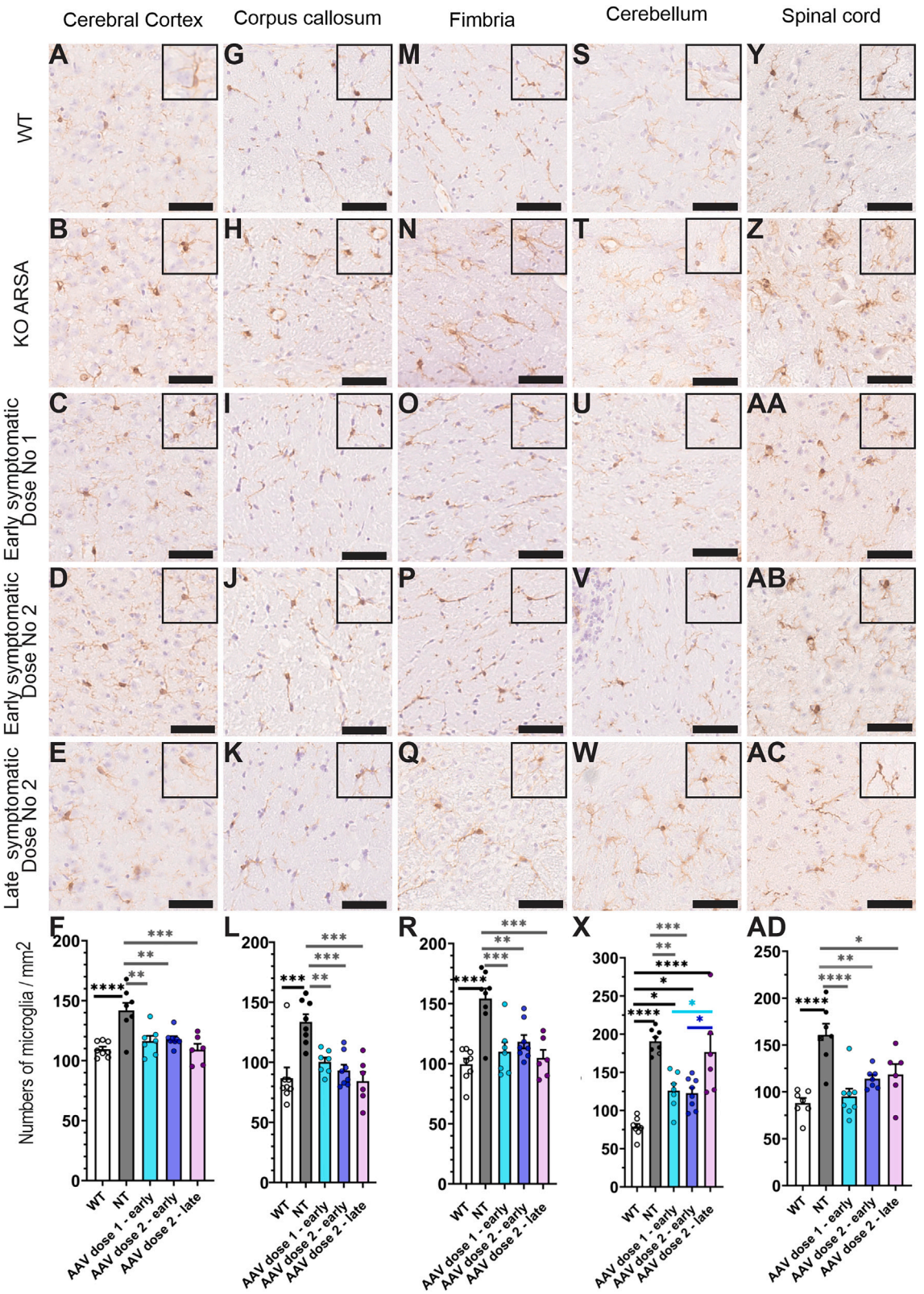

(legend on next page)

macrophages, which is a prominent feature in age-associated deep subcortical white matter lesions.[46] Consequently, in MLD mice, a population of $Iba^{-}/CD68^{+}$ microglial cells or macrophages would also be localized near sulfatide accumulations, and the number of sulfatide accumulations would be too high for the macrophages to phagocytize all of them. This population of microglial cells would be strongly present in the case of pathology or severe neuroinflammation. In contrast, the mild remaining sulfatide accumulation in the treated mice was co-localized with CD68-positive cells, between 80% and 100% depending on the area of the CNS. These macrophages are essentially microglial cells (in 50%–80% of the cases), which most probably phagocytize the remaining sulfatide aggregates. The treatment allows the role of the ARSA enzyme to be restored in the catabolism of sulfatides. This would prevent new accumulations of sulfatide in treated mice and allow sulfatide storages already present to be phagocytized thanks to the activity of microglial cells and macrophages.

Altogether, the intravenous delivery of the AAVPHP.eB-hARSA-HA vector resulted in an unprecedented level of sulfatide correction in the CNS. Those results provide strong support for implementing intravenous AAVPHP.eB gene therapy in MLD patients with rapidly progressive forms of the disease after disease onset. Previous studies in NHPs revealed the absence of the LY6 receptor, and this could impair the efficacy of AAVPHP.eB in larger animals and humans.[24,25] However, we demonstrated, using three different payloads, the efficacy of targeting the CNS with the intravenous delivery of AAVPHP.eB in NHPs.[26] Tolerance and efficacy studies are currently in progress in NHPs, in particular to evaluate the dose of AAVPHP.eB that would be required for therapeutical benefit, before the approach can be translated to human patients. Finally, the broad distribution of AAVPHP.eB could pave the way for such an approach to be applied to other LSDs. Moreover, since these data were generated, new AAV vectors with high CNS tropism in large animals, such as AAVMacPNS1,[47] have been described and are under evaluation for translational application in MLD.

MATERIALS AND METHODS

Adeno-associated viral vector construction and production

AAV vectors were produced and purified by Target (Translational Vector Core Research grade services, Nantes, France). The pAAVPHP.eB encapsidation plasmid was obtained from Addgene. The viral constructs for AAVPHP.eB-CAG-hARSA-HA contained the expression cassette consisting of the human ARSA gene followed by the human influenza hemagglutinin (HA) tag under the CAG promoter,[17] as previously described by our group.[23] The final titer of the batch was 1.1×10^{13} vector genomes (vg)/ml.

Animal model

Immunotolerant MLD mice ($mARSA^{-/-}$ hARSAC69S mice, named MLD mice), provided by Matzner Ulrich, are tolerant to human ARSA and murine ARSA KOs and were bred from heterozygous founders.[48] Mice were housed in a pathogen-free animal facility in a temperature-controlled room and maintained on a 12-h light/dark cycle. Food and water were available ad libitum.

All animal studies were performed in accordance with local and national regulations and were reviewed and approved by the relevant institutional animal care and use committee. The experiments were carried out in accordance with European Community Council Directive 2010/63/EU for the care and use of laboratory animals. Our protocol was approved by European Community Council Directive 2010/63/EU (no. 17303).

Assessment of the phenotype of MLD mice

To assess more precisely the neuropathological phenotype of the MLD mouse model, female and male MLD mice were studied in WT and KO ARSA mice aged 6 (n = 8, each group) and 9 months (WT: n = 3; KO: n = 5; Figure S1A).

Injection of the AAV vector

Mice were anesthetized with 3%–4% isoflurane and then maintained at 2% with 80% air and 20% oxygen. Treated mice were injected with AAVPHP.eB-hARSA-HA (2.5×10^{11} vg total [named dose 1] or 5×10^{11} vg total [named dose 2]) by intravenous retro-orbital delivery[49] at 6 or 9 months of age. Five groups of animals were used (Figure S1B): wild-type mice (WT, n = 15), untreated MLD mice (NT, n = 12), early-treated MLD mice with dose 1 (n = 8) or dose 2 (n = 12), and late-treated MLD mice with dose 2 (n = 6).

Tissue preparation

All animals were euthanized by an intraperitoneal administration of a lethal dose of Euthasol (180 mg/kg, Vetcare). Mice were perfused intracardially with phosphate-buffered saline (PBS). The brain, spinal cord, sciatic nerve, heart, liver, gallbladder, lungs, spleen, and kidneys were collected for analysis. Different structures of a single cerebral hemisphere (the cortex, cerebellum, pons, and rest of the brain) were dissected and frozen in liquid nitrogen. The sciatic nerve, heart, liver, lungs, spleen, and kidneys were directly frozen in liquid nitrogen and stored at −80°C. For DNA, sulfatide analysis, and protein extraction from the same samples, tissue samples were crushed in liquid nitrogen and divided into three equal parts. A single cerebral hemisphere and a portion of the spinal cord, sciatic nerve, kidneys, and gallbladder were postfixed overnight in 4% paraformaldehyde (PFA)/PBS1X. Samples were rinsed

Figure 4. Correction of microgliosis in the brain and spinal cord of treated MLD mice, 3 or 6 months after treatment

(A–E, G–K, M–Q, S–W, Y–AC) Immunohistochemistry of Iba1 in the cerebral cortex (A–E), corpus callosum (G–K), fimbria (M–Q), cerebellar white matter (S–W), and spinal cord (Y–AC) of wild-type mice (WT; A, G, M, S, and Y), untreated mice (KO ARSA; B, H, N, T, and Z), early-treated MLD mice with dose 1 (C, I, O, U, and AA) or dose 2 (D, J, P, V, and AB), and late-treated MLD mice with dose 2 (E, K, Q, W, and AC). Inserts are the high-magnification images of tissue sections. (F, L, P, R, X, and AD) Quantification of Iba1-positive cells per mm^2 in the cortex (F), corpus callosum (L), fimbria (R), cerebellar white matter (X), and spinal cord (AD) of WT, untreated (NT), and early- or late-treated MLD mice. Data are presented as mean ± SEM. Scale bars: 50 μm. *$p < 0.05$; **$p < 0.01$; ***$p < 0.005$; ****$p < 0.0001$.

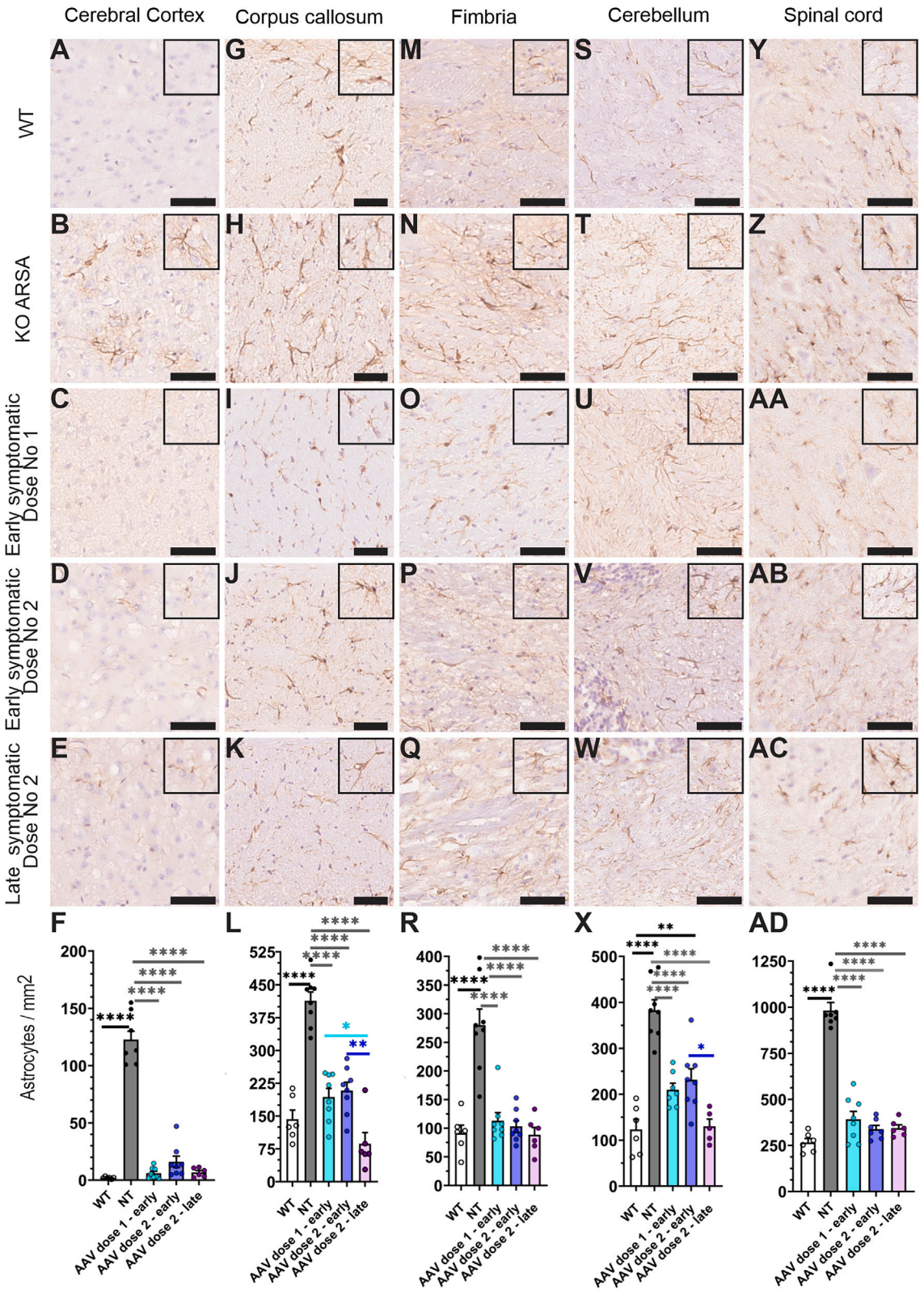

(legend on next page)

in PBS1X and cryoprotected in 30% sucrose/PBS1X. Tissues were embedded in Tissue-Tek OCT compound (VWR International) and cut into a 14-μm sagittal section (brain), a transversal section (spinal cord), a 4-μm longitudinal section (sciatic nerve and kidneys), or a transversal section (gallbladder) using a cryostat (Leica, Langham, TX). Cryosections were dried at room temperature and stored at −80°C.

Quantitative PCR

DNA was extracted from the brain, spinal cord, and peripheral organs using a chloroform and phenol protocol. AAVPHP.eB-hARSA-HA VGC numbers were measured by quantitative PCR in the cortex, cerebellum, pons, rest of the brain, spinal cord, and peripheral organs using the Light Cycler 480 SYBR Green I Master (Roche, France) as previously described.[16] The results (VGC number per cell) were expressed as *n*-fold differences in the transgene sequence copy number relative to the Adck3 gene copy number as internal standard (viral genome copy number for a 2*n* genome). Primer sequences for qPCR are available on request.

ARSA activity

Samples (tissue) were homogenized in 0.3 mL of lysis buffer (100 mM Trizma base, 150 mM NaCl, 0.3% Triton; pH 7), incubated for 30 min on ice, and centrifuged. The supernatant was collected for the determination of (1) protein content (bicinchoninic acid [BCA] protein assay kit; Pierce Biotechnology/Thermo Fisher Scientific, Rockville, IL, USA) and (2) ARSA activity, using the artificial *p*-nitrocatechol sulfate (pNCS) substrate assay (Sigma-Aldrich, France).[17,50] Assays were performed in triplicate, and results are expressed as nanomoles of 4-nitrocatechol (4NC) per hour per milligram of protein.

Mass spectrometry analysis

For sulfo-galactosylceramide analysis, we used an LC-MS/MS system comprising a QTrap 6500 mass spectrometer (ABSciex, Les Ulis, France) equipped with a Shimadzu NEXERA XR liquid chromatography system (Shimadzu, Marne La Vallée, France). The mass parameters were optimized and were as follows: an ionization voltage of 5,500 V in positive mode, a capillary temperature of 250°C, and a constant collision energy of 52. The liquid chromatography column used was a YMC-Pack PVA-Sil column (YMC, Kyoto, Japan), with an internal diameter of 3.0 mm, a porosity of 120 Å, a particle size of 5 μm, and a specific dimension of 250 mm × 3.0 mm. The elution gradient (solvent A: 58% 2-propanol, 40% hexane, and 2% ac NH_3; solvent B: 55% 2-propanol, 30% hexane, 2% ac NH_3, and 8% water) was performed at a constant flow rate of 0.5 mL/min with a starting proportion of 0% for solvent B, followed by holding at 0% for 3 min, an increase to 100% for solvent B at 7 min, and finally a return to 0% at 15 min.

After weighing, the marrow was recovered in 1 mL of NaCl solution. Using a tissue lyser (Quiagen, Les Ulis, France), the marrow samples were homogenized. After the addition of a deuterated C18 3′-sulfo-galactosylceramide-d8 (d18:1/18:0-d3) internal standard (Cayman Chemical, Ann Arbor, MI, USA), extraction was performed by adding 5 mL of a mixture of chloroform and methanol (in a ratio of 2:1) followed by a vortex step. To neutralize any acids, we added 1 mL of 0.9% NaOH solution and performed another vortex cycle. Centrifugation was then performed to separate the phases. The organic phase was carefully collected and evaporated under a nitrogen flow for 1 min. Recovery was performed by adding 200 μL of solvent A. Concentrations of the lipid compounds were determined by comparing the peak area of each complex lipid with that of the internal standard added with a known quantity. In total, 16 sulfo-galactosylceramide species were acquired using the multiple reaction monitoring transitions detailed in the supplemental table (Table S1).

Histopathology

To evaluate sulfatide storage, frozen sections were postfixed in 4% PFA, stained with Alcian blue (A5268; Sigma-Aldrich) (0.05% in 0.025 M sodium acetate buffer, pH 5.7, containing 0.3 M $MgCl_2$ and 1% PFA), rinsed in the same buffer without dye, counterstained with fast red (229113; Sigma-Aldrich), and mounted as previously described.[17]

For immunohistochemical and fluorescence labeling to study inflammation and characterize the types of cells around sulfatide aggregates, frozen sections were stained with Alcian blue as described above without counterstaining with fast red. Then immunohistochemical or fluorescence labeling could be performed as described below.

Immunohistochemical labeling was performed with the ABC method, following the protocol described by our group.[23] In some cases, slides were counterstained with hematoxylin. The slides were mounted with Eukitt (VWR International).

For immunofluorescence labeling, tissue cryosections were saturated with NGS 10%, Triton 0.3%, and PBS1X. Primary antibodies were diluted in the saturation solution and incubated overnight at 4°C. After a wash in PBS/Triton 0.1%, secondary antibodies were diluted in the saturation buffer and incubated for 1–2 h at room temperature.

Figure 5. Correction of astrogliosis in the brain and spinal cord of treated MLD mice, 3 or 6 months after treatment

(A–E, G–K, M–Q, S–W, Y–AC) Immunohistochemistry of GFAP in the cerebral cortex (A–E), corpus callosum (G–K), fimbria (M–Q), cerebellar white matter (S–W), and spinal cord (Y–AC) of wild-type mice (WT; A, G, M, S, and Y), untreated mice (KO ARSA; B, H, N, T, and Z), early-treated MLD mice with dose 1 (C, I, O, U, and AA) or dose 2 (D, J, P, V, and AB), and late-treated MLD mice with dose 2 (E, K, Q, W, and AC). Inserts are the high-magnification images of tissue sections. (F, L, P, R, X, and AD) Quantification of GFAP-positive cells per mm^2 in the cortex (F), corpus callosum (L), fimbria (R), cerebellar white matter (X), and spinal cord (AD) of WT, untreated (NT), and early- or late-treated MLD mice. Data are presented as mean ± SEM. Scale bars: 50 μm. $^*p < 0.05$; $^{**}p < 0.01$; $^{***}p < 0.005$; $^{****}p < 0.0001$.

Table 1. Sulfatide aggregate and CD68 cell quantification

	Cortex	Corpus callosum	Fimbria	Cb WM	Spinal cord
WT (n = 4)	0	0	0	0	0
	0%	0%	0%	0%	0%
NT (n = 3)	870/1072	534/1147	261/502	743/1053	607/779
	81.15%	45.68%	52%	70.5%	77.92%
AAV dose 1 – early (n = 3)	0	17/17	43/43	13/13	35/35
	0%	100%	100%	100%	100%
AAV dose 2 – early (n = 3)	0	25/25	20/20	6/6	13/13
	0%	100%	100%	100%	100%
AAV dose 2 – late (n = 3)	9/11	249/276	88/110	110/121	72/77
	81.81%	90.21%	80%	91%	93.51%

Table showing the number of sulfatide aggregates and CD68-positive cells over the total number of sulfatide storages counted, as well as the percentage, for each group of mice in different structures of the CNS (cortex, corpus callosum, fimbria, cerebellar white matter [Cb WM]) and spinal cord.

After washing with PBS, slides were mounted with DAPI Fluoromount (#0100-20; SouthernBiotech).

The following primary antibodies were used: mouse anti-GFAP (G3893, Sigma-Aldrich; 1:400), rabbit anti-Iba1 (019–19741, WAKO; 1:750), and rat anti-CD68 (MCA1957, Bio-Rad; 1:200).

The following secondary antibodies were used: biotinylated goat anti-rabbit (BA-1000, Vector Lab; 1:1,000), biotinylated goat anti-mouse (BA9200, Vector Lab; 1:1,000), biotinylated goat anti-rat (BA9400, Vector Lab; 1:1,000), goat anti-rabbit Alexa Fluor 488 (A11034, Life Technologies; 1:1,000), and goat anti-rat Alexa Fluor 594 (A11007, Life Technologies; 1:1,000).

BaseScope

All steps were done in an RNase-free space and with sterilized materials when possible. After validation of the quality of mRNA in our tissues with a positive and a negative control (ref. nos. 712351 and 701021, Advanced Cell Diagnostics), the BaseScope experiment was done with the BaseScope Detection Reagent Kit v2 – RED (cat. no. 323900). Briefly, after drying and dehydration in a fresh ethanol solution, RNAscope hydrogen peroxide (322335, Advanced Cell Diagnostics) was applied for 10 min at room temperature. After two washes in distilled water, a protease III solution was applied (322340, Advanced Cell Diagnostics), and slides were incubated for 15 min at 40°C in an ACD HybEZ Hybridization System (cat. nos. 310010 and 310013, Advanced Cell Diagnostics). Then, the probe of interest (designed to be specific to the transgene sequence and not to endogenous hARSA), the BaseScope Probe BA-Hs-ARSAHA-Junc-C1 (1234091-C1, Advanced Cell Diagnostics), was hybridized for 2 h at 40°C and washed in an RNAscope wash buffer reagent (310091, Advanced Cell Diagnostics). Amplification and revelation of the signal were performed as described in the BaseScope Detection Reagent Kit v2 – RED User Manual (document number 323900-USM, Advanced Cell Diagnostics), except for the 7th amplification, which was reduced from 30 to 20 min at room temperature in order to diminish the signal, which was too strong in our previous tests. After washing, slides were dipped in a 0.1% toluidine solution for 10 to 15 s (185426, Sigma-Aldrich) for a light counterstaining and then mounted with Ecomount (320409, Advanced Cell Diagnostics).

All slices were acquired at 40× magnification by using a slide scanner (NanoZoomerS60, Hamamatsu, or an Axio Scan.Z1, Carl Zeiss). Some pictures were taken with an Apotome 2 ZEISS upright widefield (Leica). For all images, brightness and contrast were adjusted with the ImageJ software after acquisition to match the observation as best as possible.

Stereological cell counts

Stereological counts were performed by two independent investigators, using ImageJ, Photoshop, or Zen software. All quantifications were done in three sections for each tissue and for each animal. For Alcian blue staining, the number of sulfatide storage inclusions was quantified and reported per quantified area in mm^2 in three random areas of the cortex, corpus callosum, fimbria, cerebellar white matter, sciatic nerve, and kidneys. For the gallbladder, the area of Alcian blue staining relative to the total epithelial cell area was quantified. For GFAP and Iba1 labeling, the number of positive cells was evaluated in three random areas of the cerebral cortex, the corpus callosum, the fimbria, and the center of the cerebellar white matter and were reported per quantified area.

In the spinal cord, for GFAP, three random areas of the spinal cord were counted. In the spinal cord, for sulfatide storage and Iba1, a hemi-section was counted. All results were assessed per mm^2 and expressed as the mean ± standard error of the mean (SEM).

Statistical analysis

Data were analyzed using GraphPad Prism 8 software. The statistical significance of values among groups was evaluated by ANOVA, followed by the least significant difference t test. All values given in the figures and text are expressed as mean ± SEM. Differences were considered significant at $p < 0.05$.

DATA AND CODE AVAILABILITY

All data are available upon motivated request.

SUPPLEMENTAL INFORMATION

Supplemental information can be found online at https://doi.org/10.1016/j.omtm.2024.101248.

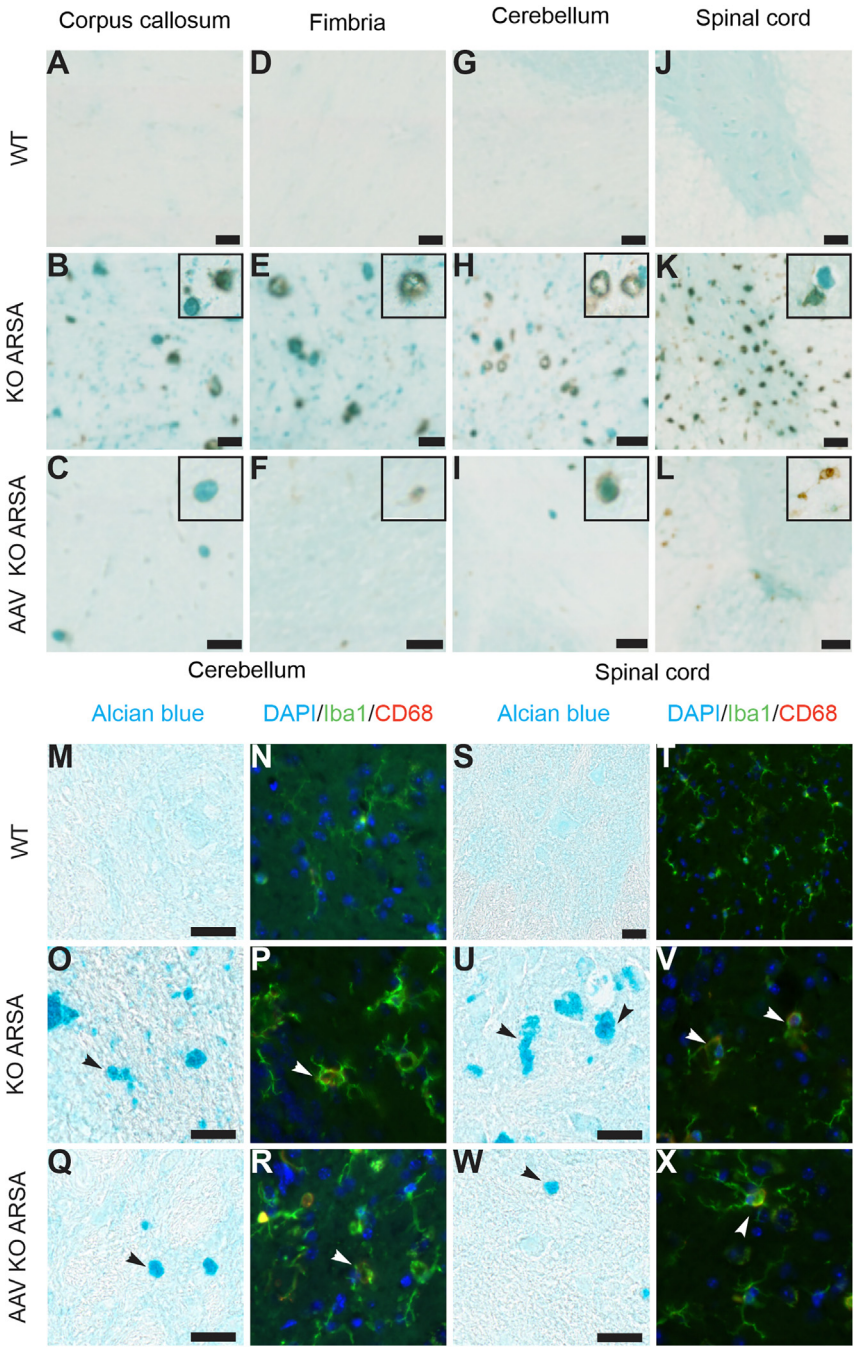

Figure 6. Sulfatide storage and macrophage and/or microglial cell staining in the brain and spinal cord of treated MLD mice, 3 or 6 months after treatment

(A–L) Immunohistochemistry of CD68 and Alcian blue staining in the corpus callosum (A–C), fimbria (D–F), cerebellar white matter (G–I), and spinal cord (J–L) of wild-type mice (WT; A, D, G, and J), untreated mice (KO ARSA; B, E, H, and K), and treated MLD mice (C, F, I, and L). Inserts are the high-magnification images of tissue sections. (M–X) Alcian blue staining followed by immunofluorescence of CD68 (red) and Iba1 (green) in the cerebellar white matter (M–R) and spinal cord (S–X) of wild-type mice (WT; M–N and S–T), untreated mice (KO ARSA; O–D and U–V), and treated MLD mice (Q–R and W–X). Arrows indicate sulfatide aggregates, which are co-localized with CD68 and Iba1. Scale bars: 20 μm (A–I), 50 μm (J–L), and 25 μm (M–X).

ACKNOWLEDGMENTS

We thank the people of the TIDU GENOV lab for materials, technical support, and discussions. We thank the people from Target facility Nantes for vector cloning and production. All animal work was conducted at the PHENO-ICMice facility. Thanks to Nadège Sarrazin and Joanna Droesbeke of PHENO-ICMice facility for animal necropsies. This work was carried out at the Histomics core facility of the ICM, and we thank all technical staff involved. We also thank Dr. Ulrich Matzner and Pr. Volkmar Gieselmann for the hARSA antibodies and recombinant ARSA supply.

This project received funding from the ELA program under grant agreement no. 2018-019I2 and Janssen Horizon funding. The research leading to these results has received funding from the

Table 2. Sulfatide aggregate and Iba1 and CD68 cell quantification

	Cortex	Corpus callosum	Fimbria	Cb WM	Spinal cord	Overall
WT (n = 4)	0	0	0	0	0	
	0%	0%	0%	0%	0%	**0%**
NT (n = 3)	187/332	95/281	37/166	94/190	115/401	
	56.33%	**33.81%**	**22.29%**	**49.47%**	**28.68%**	**38.11%**
AAV dose 1 – early (n = 3)	2/11	65/67	23/25	44/61	13/14	
	18.2%	**84.42%**	**92%**	**72.13%**	**92.86%**	**71.92%**
AAV dose 2 – early (n = 3)	0	33/57	4/5	12/20	2/3	
	0%	**57.89%**	**80%**	**60%**	**66.66%**	**52.91%**
AAV dose 2 – late (n = 3)	9/11	219/276	67/110	110/121	51/77	
	81.82%	**79.35%**	**60.91%**	**84.3%**	**66.23%**	**74.52%**

Table showing the number of sulfatide aggregates that also contain CD68-and Iba1-positive cells over the total number of sulfatide storages counted, as well as the percentage, for each group of mice in different structures of the CNS (cortex, corpus callosum, fimbria, cerebellar white matter [Cb WM]) and spinal cord.

program "Investissements d'avenir" ANR-10- IAIHU-06 and ANR-11- INBS-0011 – NeurATRIS: Translational Research Infrastructure for Biotherapies in Neurosciences.

AUTHOR CONTRIBUTIONS

E.A. and F.P. designed the experiments. E.A., F.P., C.M., N.K., C.L., E.-G.B., and A.L. performed experiments. E.A., F.P., and C.S. wrote the paper.

DECLARATION OF INTERESTS

No conflicts of interest is declare

REFERENCES

1. Gieselmann, V., and Krägeloh-Mann, I. (2006). Metachromatic Leukodystrophy. In Scriver's Online Metabolic and Molecular Bases of Inherited Disease, C.R. Scriver, A.L. Beaudet, W.S. Sly, D. Valle, B. Childs, K.W. Kinzler, and B. Vogelstein, eds. https://doi.org/10.1036/ommbid.179.
2. Parikh, S., Bernard, G., Leventer, R.J., van der Knaap, M.S., van Hove, J., Pizzino, A., McNeill, N.H., Helman, G., Simons, C., Schmidt, J.L., et al. (2015). A clinical approach to the diagnosis of patients with leukodystrophies and genetic leukoencephalopathies. Mol. Genet. Metab. *114*, 501–515. https://doi.org/10.1016/J.YMGME.2014.12.434.
3. Gieselmann, V., and Krägeloh-Mann, I. (2010). Metachromatic leukodystrophy an update. Neuropediatrics *41*, 1–6. https://doi.org/10.1055/s-0030-1253412.
4. Van Rappard, D.F., Boelens, J.J., and Wolf, N.I. (2015). Metachromatic leukodystrophy: Disease spectrum and approaches for treatment. Best Pract. Res. Clin. Endocrinol. Metab. *29*, 261–273. https://doi.org/10.1016/j.beem.2014.10.001.
5. Shaimardanova, A.A., Chulpanova, D.S., Solovyeva, V.V., Mullagulova, A.I., Kitaeva, K.V., Allegrucci, C., and Rizvanov, A.A. (2020). Metachromatic Leukodystrophy: Diagnosis, Modeling, and Treatment Approaches. Front. Med. *7*, 692. https://doi.org/10.3389/FMED.2020.576221/BIBTEX.
6. Í Dali, C., Sevin, C., Krägeloh-Mann, I., Giugliani, R., Sakai, N., Wu, J., and Wasilewski, M. (2020). Safety of intrathecal delivery of recombinant human arylsulfatase A in children with metachromatic leukodystrophy: Results from a phase 1/2 clinical trial. Mol. Genet. Metab. *131*, 235–244. https://doi.org/10.1016/j.ymgme.2020.07.002.
7. Biffi, A., Montini, E., Lorioli, L., Cesani, M., Fumagalli, F., Plati, T., Baldoli, C., Martino, S., Calabria, A., Canale, S., et al. (2013). Lentiviral hematopoietic stem cell gene therapy benefits metachromatic leukodystrophy. Science *341*, 1233158. https://doi.org/10.1126/science.1233158.
8. Sessa, M., Lorioli, L., Fumagalli, F., Acquati, S., Redaelli, D., Baldoli, C., Canale, S., Lopez, I.D., Morena, F., Calabria, A., et al. (2016). Lentiviral haemopoietic stem-cell gene therapy in early-onset metachromatic leukodystrophy: an ad-hoc analysis of a non-randomised, open-label, phase 1/2 trial. Lancet *388*, 476–487. https://doi.org/10.1016/S0140-6736(16)30374-9.
9. Fumagalli, F., Calbi, V., Natali Sora, M.G., Sessa, M., Baldoli, C., Rancoita, P.M.V., Ciotti, F., Sarzana, M., Fraschini, M., Zambon, A.A., et al. (2022). Lentiviral haematopoietic stem-cell gene therapy for early-onset metachromatic leukodystrophy: long-term results from a non-randomised, open-label, phase 1/2 trial and expanded access. Lancet (London, England) *399*, 372–383. https://doi.org/10.1016/S0140-6736(21)02017-1.
10. Sevin, C., Roujeau, T., Cartier, N., Baugnon, T., Adamsbaum, C., Piraud, M., Martino, S., Mouiller, P., Couzinié, C., Bellesme, C., et al. (2018). Intracerebral gene therapy in children with metachromatic leukodystrophy: Results of a phase I/II trial. Mol. Genet. Metab. *123*, S129. https://doi.org/10.1016/j.ymgme.2017.12.352.
11. Platt, F.M., and Lachmann, R.H. (2009). Treating lysosomal storage disorders: Current practice and future prospects. Biochim. Biophys. Acta *1793*, 737–745. https://doi.org/10.1016/j.bbamcr.2008.08.009.
12. Matthes, F., Wölte, P., Böckenhoff, A., Hüwel, S., Schulz, M., Hyden, P., Fogh, J., Gieselmann, V., Galla, H.J., and Matzner, U. (2011). Transport of arylsulfatase A across the blood-brain barrier in vitro. J. Biol. Chem. *286*, 17487–17494. https://doi.org/10.1074/jbc.M110.189381.
13. Matzner, U., Lüllmann-Rauch, R., Stroobants, S., Andersson, C., Weigelt, C., Eistrup, C., Fogh, J., D'Hooge, R., and Gieselmann, V. (2009). Enzyme Replacement Improves Ataxic Gait and Central Nervous System Histopathology in a Mouse Model of Metachromatic Leukodystrophy. Mol. Ther. *17*, 600–606. https://doi.org/10.1038/mt.2008.305.
14. Rosenberg, J.B., Kaminsky, S.M., Aubourg, P., Crystal, R.G., and Sondhi, D. (2016). Gene therapy for metachromatic leukodystrophy. J. Neurosci. Res. *94*, 1169–1179. https://doi.org/10.1002/jnr.23792.
15. Abbott, N.J. (2013). Blood-brain barrier structure and function and the challenges for CNS drug delivery. J. Inherit. Metab. Dis. *36*, 437–449. https://doi.org/10.1007/S10545-013-9608-0.
16. Sevin, C., Benraiss, A., Van Dam, D., Bonnin, D., Nagels, G., Verot, L., Laurendeau, I., Vidaud, M., Gieselmann, V., Vanier, M., et al. (2006). Intracerebral adeno-associated virus-mediated gene transfer in rapidly progressive forms of metachromatic leukodystrophy. Hum. Mol. Genet. *15*, 53–64. https://doi.org/10.1093/hmg/ddi425.

17. Piguet, F., Sondhi, D., Piraud, M., Fouquet, F., Hackett, N.R., Ahouansou, O., Vanier, M.T., Bieche, I., Aubourg, P., Crystal, R.G., et al. (2012). Correction of brain oligodendrocytes by AAVrh.10 intracerebral gene therapy in metachromatic leukodystrophy mice. Hum. Gene Ther. *23*, 903–914. https://doi.org/10.1089/hum.2012.015.

18. Sevin, C., Verot, L., Benraiss, A., Van Dam, D., Bonnin, D., Nagels, G., Fouquet, F., Gieselmann, V., Vanier, M.T., De Deyn, P.P., et al. (2007). Partial cure of established disease in an animal model of metachromatic leukodystrophy after intracerebral adeno-associated virus-mediated gene transfer. Gene Ther. *14*, 405–414. https://doi.org/10.1038/sj.gt.3302883.

19. Colle, M.A., Piguet, F., Bertrand, L., Raoul, S., Bieche, I., Dubreil, L., Sloothaak, D., Bouquet, C., Moullier, P., Aubourg, P., et al. (2010). Efficient intracerebral delivery of AAV5 vector encoding human ARSA in non-human primate. Hum. Mol. Genet. *19*, 147–158. https://doi.org/10.1093/hmg/ddp475.

20. Zerah, M., Piguet, F., Colle, M.A., Raoul, S., Deschamps, J.Y., Deniaud, J., Gautier, B., Toulgoat, F., Bieche, I., Laurendeau, I., et al. (2015). Intracerebral Gene Therapy Using AAVrh.10-hARSA Recombinant Vector to Treat Patients with Early-Onset Forms of Metachromatic Leukodystrophy: Preclinical Feasibility and Safety Assessments in Nonhuman Primates. Hum. Gene Ther. Clin. Dev. *26*, 113–124. https://doi.org/10.1089/humc.2014.139.

21. Miyake, N., Miyake, K., Sakai, A., Yamamoto, M., Suzuki, H., and Shimada, T. (2021). Treatment of adult metachromatic leukodystrophy model mice using intrathecal administration of type 9 AAV vector encoding arylsulfatase A. Sci. Rep. *11*, 20513. https://doi.org/10.1038/S41598-021-99979-2.

22. Chan, K.Y., Jang, M.J., Yoo, B.B., Greenbaum, A., Ravi, N., Wu, W.L., Sánchez-Guardado, L., Lois, C., Mazmanian, S.K., Deverman, B.E., and Gradinaru, V. (2017). Engineered AAVs for efficient noninvasive gene delivery to the central and peripheral nervous systems. Nat. Neurosci. *20*, 1172–1179. https://doi.org/10.1038/nn.4593.

23. Audouard, E., Oger, V., Meha, B., Cartier, N., Sevin, C., and Piguet, F. (2021). Complete Correction of Brain and Spinal Cord Pathology in Metachromatic Leukodystrophy Mice. Front. Mol. Neurosci. *14*, 677895. https://doi.org/10.3389/fnmol.2021.677895.

24. Huang, Q., Chan, K.Y., Tobey, I.G., Chan, Y.A., Poterba, T., Boutros, C.L., Balazs, A.B., Daneman, R., Bloom, J.M., Seed, C., and Deverman, B.E. (2019). Delivering genes across the blood-brain barrier: LY6A, a novel cellular receptor for AAV-PHP.B capsids. PLoS One *14*, e0225206. https://doi.org/10.1371/journal.pone.0225206.

25. Hordeaux, J., Yuan, Y., Clark, P.M., Wang, Q., Martino, R.A., Sims, J.J., Bell, P., Raymond, A., Stanford, W.L., and Wilson, J.M. (2019). The GPI-Linked Protein LY6A Drives AAV-PHP.B Transport across the Blood-Brain Barrier. Mol. Ther. *27*, 912–921. https://doi.org/10.1016/J.YMTHE.2019.02.013.

26. Piguet, F., and Sevin, C. (2023). RECOMBINANT AAV VECTORS FOR TREATING NERVOUS SYSTEM DISEASES. US patent 17749501.

27. Hess, B., Saftig, P., Hartmann, D., Coenen, R., Lüllmann-Rauch, R., Goebel, H.H., Evers, M., Von Figura, K., D'Hooge, R., Nagels, G., et al. (1996). Phenotype of arylsulfatase A-deficient mice: Relationship to human metachromatic leukodystrophy. Proc. Natl. Acad. Sci. USA *93*, 14821–14826. https://doi.org/10.1073/pnas.93.25.14821.

28. Stein, A., Stroobants, S., Gieselmann, V., D'Hooge, R., and Matzner, U. (2015). Anti-inflammatory therapy with simvastatin improves neuroinflammation and CNS function in a mouse model of metachromatic leukodystrophy. Mol. Ther. *23*, 1160–1168. https://doi.org/10.1038/mt.2015.69.

29. Jeon, S.-B., Yoon, H.J., Park, S.-H., Kim, I.-H., and Park, E.J. (2008). Sulfatide, A Major Lipid Component of Myelin Sheath, Activates Inflammatory Responses As an Endogenous Stimulator in Brain-Resident Immune Cells. J. Immunol. *181*, 8077–8087. https://doi.org/10.4049/jimmunol.181.11.8077.

30. Takahashi, T., and Suzuki, T. (2012). Role of sulfatide in normal and pathological cells and tissues. J. Lipid Res. *53*, 1437–1450. https://doi.org/10.1194/JLR.R026682.

31. Von Figura, K., Gieselmann, V., and Jaeken, J. (2001). Metachromatic leukodystrophy. In Metab. Mol. Bases Inherit. Dis. 8th, C. Scriver, A. Beaudet, W. Sly, and D. Valle, eds. (McGraw-Hill), pp. 3695–3724.

32. Wittke, D., Hartmann, D., Gieselmann, V., and Lüllmann-Rauch, R. (2004). Lysosomal sulfatide storage in the brain of arylsulfatase A-deficient mice: Cellular alterations and topographic distribution. Acta Neuropathol. *108*, 261–271. https://doi.org/10.1007/s00401-004-0883-6.

33. Í Dali, C., Groeschel, S., Moldovan, M., Farah, M.H., Krägeloh-Mann, I., Wasilewski, M., Li, J., Barton, N., and Krarup, C. (2021). Intravenous arylsulfatase A in metachromatic leukodystrophy: a phase 1/2 study. Ann. Clin. Transl. Neurol. *8*, 66–80. https://doi.org/10.1002/acn3.51254.

34. Mullagulova, A., Shaimardanova, A., Solovyeva, V., Mukhamedshina, Y., Chulpanova, D., Kostennikov, A., Issa, S., and Rizvanov, A. (2023). Safety and Efficacy of Intravenous and Intrathecal Delivery of AAV9-Mediated ARSA in Minipigs. Int. J. Mol. Sci. *24*, 9204. https://doi.org/10.3390/IJMS24119204.

35. Ertl, H.C.J. (2023). Mitigating Serious Adverse Events in Gene Therapy with AAV Vectors: Vector Dose and Immunosuppression. Drugs *83*, 287–298. https://doi.org/10.1007/S40265-023-01836-1.

36. Chand, D., Mohr, F., McMillan, H., Tukov, F.F., Montgomery, K., Kleyn, A., Sun, R., Tauscher-Wisniewski, S., Kaufmann, P., and Kullak-Ublick, G. (2021). Hepatotoxicity following administration of onasemnogene abeparvovec (AVXS-101) for the treatment of spinal muscular atrophy. J. Hepatol. *74*, 560–566. https://doi.org/10.1016/J.JHEP.2020.11.001.

37. Ziegler, A., Wilichowski, E., Schara, U., Hahn, A., Müller-Felber, W., Johannsen, J., von der Hagen, M., von Moers, A., Stoltenburg, C., Saffari, A., et al. (2020). [Recommendations for gene therapy of spinal muscular atrophy with onasemnogene abeparvovec-AVXS-101 : Consensus paper of the German representatives of the Society for Pediatric Neurology (GNP) and the German treatment centers with collaboration of the medical scientific advisory board of the German Society for Muscular Diseases (DGM)]. Nervenarzt *91*, 518–529. https://doi.org/10.1007/S00115-020-00919-8.

38. Matthes, F., Stroobants, S., Gerlach, D., Wohlenberg, C., Wessig, C., Fogh, J., Gieselmann, V., Eckhardt, M., D'Hooge, R., and Matzner, U. (2012). Efficacy of enzyme replacement therapy in an aggravated mouse model of metachromatic leukodystrophy declines with age. Hum. Mol. Genet. *21*, 2599–2609. https://doi.org/10.1093/hmg/dds086.

39. Isaac, G., Pernber, Z., Gieselmann, V., Hansson, E., Bergquist, J., and Månsson, J.E. (2006). Sulfatide with short fatty acid dominates in astrocytes and neurons. FEBS J. *273*, 1782–1790. https://doi.org/10.1111/j.1742-4658.2006.05195.x.

40. Holness, C.L., Da Silva, R.P., Fawcett, J., Gordon, S., and Simmons, D.L. (1993). Macrosialin, a mouse macrophage-restricted glycoprotein, is a member of the lamp/lgp family. J. Biol. Chem. *268*, 9661–9666. https://doi.org/10.1016/s0021-9258(18)98400-0.

41. Holness, C.L., and Simmons, D.L. (1993). Molecular Cloning of CD68, a Human Macrophage Marker Related to Lysosomal Glycoproteins. Blood *81*, 1607–1613. https://doi.org/10.1182/BLOOD.V81.6.1607.1607.

42. Chistiakov, D.A., Killingsworth, M.C., Myasoedova, V.A., Orekhov, A.N., and Bobryshev, Y.V. (2017). CD68/macrosialin: not just a histochemical marker. Lab. Invest. *97*, 4–13. https://doi.org/10.1038/LABINVEST.2016.116.

43. Fu, R., Shen, Q., Xu, P., Luo, J.J., and Tang, Y. (2014). Phagocytosis of microglia in the central nervous system diseases. Mol. Neurobiol. *49*, 1422–1434. https://doi.org/10.1007/S12035-013-8620-6.

44. Poppell, M., Hammel, G., and Ren, Y. (2023). Immune Regulatory Functions of Macrophages and Microglia in Central Nervous System Diseases. Int. J. Mol. Sci. *24*, 5925. https://doi.org/10.3390/ijms24065925.

45. Walker, D.G., and Lue, L.F. (2015). Immune phenotypes of microglia in human neurodegenerative disease: challenges to detecting microglial polarization in human brains. Alzheimer's Res. Ther. *7*, 56. https://doi.org/10.1186/S13195-015-0139-9.

46. Waller, R., Baxter, L., Fillingham, D.J., Coelho, S., Pozo, J.M., Mozumder, M., Frangi, A.F., Ince, P.G., Simpson, J.E., and Highley, J.R. (2019). Iba-1-/CD68+

microglia are a prominent feature of age-associated deep subcortical white matter lesions. PLoS One *14*, e0210888. https://doi.org/10.1371/JOURNAL.PONE.0210888.

47. Chuapoco, M.R., Flytzanis, N.C., Goeden, N., Christopher Octeau, J., Roxas, K.M., Chan, K.Y., Scherrer, J., Winchester, J., Blackburn, R.J., Campos, L.J., et al. (2023). Adeno-associated viral vectors for functional intravenous gene transfer throughout the non-human primate brain. Nat. Nanotechnol. *18*, 1241–1251. https://doi.org/10.1038/S41565-023-01419-X.

48. Matzner, U., Matthes, F., Herbst, E., Lüllmann-Rauch, R., Callaerts-Vegh, Z., D'Hooge, R., Weigelt, C., Eistrup, C., Fogh, J., and Gieselmann, V. (2007). Induction of tolerance to human arylsulfatase A in a mouse model of metachromatic leukodystrophy. Mol. Med. *13*, 471–479. https://doi.org/10.2119/2007-00063.Matzner.

49. Yardeni, T., Eckhaus, M., Morris, H.D., Huizing, M., and Hoogstraten-Miller, S. (2011). Retro-orbital injections in mice. Lab Anim. (NY) *40*, 155–160. https://doi.org/10.1038/laban0511-155.

50. Bass, N.H., Witmer, E.J., and Dreifuss, F.E. (1970). A Pedigree studv of metachromatic leukodystrophy: Biochemical identification of the carrier state. Neurology *20*, 52–62. https://doi.org/10.1212/wnl.20.1.52.